Analyst

PAPER

View Article Online
View Journal

Cite this: DOI: 10.1039/c6an00069j

pulSED: pulsed sonoelectrodeposition of fractal nanoplatinum for enhancing amperometric biosensor performance†

M. Taguchi,[a] N. Schwalb,[a] Y. Rong,[a] D. C. Vanegas,[a,b] N. Garland,[c] M. Tan,[d] H. Yamaguchi,[d] J. C. Claussen[c] and E. S. McLamore*[a]

Received 10th January 2016,
Accepted 20th April 2016

DOI: 10.1039/c6an00069j

www.rsc.org/analyst

For the first time, we combine pulsed electrodeposition with out-of-phase pulsed sonication for controlled synthesis of fractal nanoplatinum structures as the transducer layer in electrochemical sensing. We develop and test this technique, called bimodal pulsed sonoelectrodeposition (pulSED), as a simple approach for creating highly conductive transducer nanometals for use in sensing and biosensing. We first compared the efficiency of pulSED nanoplatinum to other pulsed electrodeposition techniques, and then explored the effect of duty cycle and plating time on electroactive surface area and nanoparticle size/morphology. The developed pulSED nanoplatinum displayed fractal features with a relatively homogenous size distribution (26.31 ± 1.3 nm) and extremely high electroactive surface (0.28 ± 0.04 cm^2) relative to other electroplating techniques (up to one order of magnitude higher). A high duty cycle (900 mHz) promotes formation of stable nanostructures (including fractal nanostructures) and reduces amorphous structure formation due to bubble cavitation and enhanced mass transport of metal ions to the electrode surface. To demonstrate the applicability of the pulSED technique, non-enzymatic and enzymatic sensors were developed for measuring hydrogen peroxide and glucose. The sensitivity for non-enzymatic peroxide sensing (3335 ± 305 μA cm^{-2} mM^{-1}), non-enzymatic glucose sensing (73 ± 14 μA cm^{-2} mM^{-1}) and enzymatic glucose biosensing (155 ± 25 μA cm^{-2} mM^{-1}) was higher than, or similar to, other nanomaterial-mediated amperometric sensors reported in the literature. The pulSED technique is a one pot method for tunable synthesis of nanometal structures as a transducer layer in electrochemical sensing and biosensing that requires no precursors or capping agents, and can be carried out at room temperature with inexpensive hardware.

Introduction

Metal nanostructures are commonly used as transducer materials for improving performance of electrochemical sensors and biosensors.[1–5] Among the many examples, some of the most common nanometal work has focused on the deposition of palladium,[6] platinum,[7,8] gold,[9,10] nickel,[11] and copper[12] *via* templated and non-templated deposition techniques.[13] These and other nanometals have been deposited on a variety of surfaces, including noble metal electrodes,[14] glassy carbon,[15] nanocarbon (*e.g.*, multilayered graphene, carbon nanotubes),[6–8] and silicon,[16] and used as a transducer layer in electrochemical sensing.

Within the various morphologies of nanometal, many groups have recently focused on the development of fractal, or self-similar, nanostructures. The impetus in development of fractal nanostructures is a form of biomimicry; natural systems have evolved fractal patterns that optimize mass transfer, heat transfer, and structural integrity.[17,18] As noted by Banavar,[19] any fractal pattern is the result of transport optimization, where the energy represents a functional component that is minimized for the transport of system fluxes. Nanoplatinum fractal structures have been developed which resemble flowers,[20–22] nanocorals, urchins,[23,24] mulberries,[25] raspberries,[26] and cauliflowers.[27] Many other metals have been used to prepare suspended and surface-deposited structures (wires, cages, *etc.*). In this manuscript we focus on the use of surface-deposited nanometal as the transducer layer for electrochemical sensing.

[a]*Department of Agricultural & Biological Engineering, Institute of Food & Agricultural Sciences, University of Florida, USA. E-mail: emclamor@ufl.edu*
[b]*Department of Food Engineering, Universidad del Valle, Colombia*
[c]*Department of Mechanical Engineering, Iowa State University, USA*
[d]*Department of Mechanical and Aerospace Engineering, University of Florida, USA*
†Electronic supplementary information (ESI) available. See DOI: 10.1039/c6an00069j

Common nanometal deposition methods include chemical vapor deposition (CVD),[23] sputtering,[28] galvanic displacement,[16,29,30] and electrodeposition.[31] Although CVD and sputtering are industry standards, electrodeposition (ED) persists as a competitive fabrication technique due to the simplicity, relatively low cost, and formation of thin films or nanostructures with high electroactive surface area. Platinum, and in particular nanoplatinum, is one of the most widely studied structures formed by electrodeposition due to its favorable electrocatalytic properties that are well-suited for many applications such as sensing,[32] fuel cell development,[33,34] and aqueous micro propulsion systems,[24,35,36] to name a few. One of the most exciting applications of nanoplatinum is the development of non-enzymatic sensors for measuring glucose, so-called third generation glucose sensors (reviewed by Park *et al.*[37]).

Kloke *et al.* and other groups have reviewed ED methods for controlling platinum size and shape for use in preparation of suspended or surface-deposited nanoplatinum.[3] ED methods for deposition of nanoplatinum generally involve careful regulation of temperature and precursor concentration, addition of exogenous reducing agents, or addition of capping agents to stop metal nucleation. In general, nanoparticle size decreases with increasing nucleation rate in relation to the crystal growth rate; thus higher temperature or concentration of reducing agents increases nucleation rate and leads to smaller nanoparticle size. However, ED in bulk solution using standard potentiostatic or galvanostatic methods produces an array of nanoparticle sizes and morphologies due to the progressive generation (rather than instantaneous formation) of nucleation sites. Since ED is often diffusion limited, control of nanometal morphology is particularly challenging, which has resulted in a bottleneck in terms of engineering highly stable transducer layers. Due to the close proximity of biorecognition elements (*e.g.*, proteins, DNA, *etc.*) and nanometal structures in biosensing, the ability to exhibit control over the morphology and size of nanometal structures is vital for fabricating efficient biosensors.

Pulsed electrodeposition (PED) is a technique that has recently gained much attention for deposition of nanometals onto conductive surfaces or nanocarbon defect sites.[38] With PED, a high overvoltage (high current density) is used in the same fashion as classic ED, but the driving potential is applied for short time periods (typically less than 1 s). During the relaxation period (*i.e.*, non-plating time period), dissolved metal ions migrate to the surface where ion consumption is highest (*i.e.*, high local current density), resulting in a more uniform distribution of metal compared to standard potentiostatic or galvanostatic ED.[39] As reviewed by Kloke *et al.*, PED has advantages over traditional ED, namely the relatively high localized concentration of dissolved metal species during the relaxation time results in a higher crystal grain and electroactive surface area.[3] If the duty cycles are controlled properly, diffusion limitations can be reduced using PED.[40] One of the most common problems with ED is uncontrolled "overgrowth" of dendritic structures beyond the working diameter of the electrode.

Another technique used to synthesize metal nanoparticles is sonochemical electrodeposition (SED). SED combines galvanostatic or potentiostatic ED with sonication. SED has primarily been used for synthesizing suspended nanoparticles,[41] including platinum,[42] copper,[43] gold,[44] CdSe nanotubes,[45] and conductive polymers such as polyaniline.[46] SED reduces diffusion limitations by facilitating acoustic cavitation and microjetting effects at the surface of the nucleating metal structure, destabilizing bubbles formed during the deposition process and also providing some convective mixing of dissolved metal ions within the mass boundary layer.[41,47] However, like PED, SED is hampered by diffusion limitations to the surface and control over nanoparticle size has not yet been demonstrated.

To date, no previous methodologies have combined PED and SED using a bimodal pulsing strategy for deposition of nanometal onto electrodes. Here, we develop this technique, called pulsed sonoelectrodeposition (pulSED), and demonstrate deposition of fractal nanoplatinum structures for electrochemical sensing and biosensing (see ESI Fig. S1†). We have recently shown the diverse applicability of the pulSED technique by depositing nanoplatinum on reduced graphene oxide[30] or nanoceria,[29] but this is the first time the technique has been studied in detail beyond proof of principle demonstrations. We first compare the electroactive surface area, nanoparticle size, and morphology of nanometals formed using pulSED and four other published techniques. Next, we explore the effect of total plating time and duty cycle (*i.e.*, deposition/relaxation rate) on nanometal morphology and electrochemical behavior using the pulSED technique. Finally, we demonstrate the development of non-enzymatic sensors (hydrogen peroxide and glucose) as well as an enzymatic biosensor (glucose) based on a fractal nanoplatinum transducer layer fabricated using the pulSED system.

Materials and methods

Chemicals, reagents, and components

Platinum/iridium electrodes (Pt/Ir, BASi MF-2013, 1.6 mm diameter, 7.5 cm length, 6 mm shaft diameter, CTFE plastic body) were purchased from BASi Inc. (West Lafayette, IN). Pt wire (99.95% Pt, 1.2 mm dia, 2 cm length) for counter electrodes was obtained from Alfa Aesar (Ward Hill, MA). Polycrystalline diamond suspensions (1 μm and 3 μm) and alumina slurry (0.05 μm) were obtained from Buehler (Lake Bluff, IL). Lead acetate (30% w/v) was purchased from Fisher Scientific (Pittsburgh, PA). Chloroplatinic acid (8 wt%), glucose oxidase, glucose, ascorbic acid, 4-aceaminophen, uric acid and hydrogen peroxide (35% wt%) were procured from Sigma-Aldrich (St Louis, MO). Potassium ferrocyanide trihydrate ($K_3FE(CN)_6$) was purchased from EMD chemicals (Billerica, USA). Potassium nitrate (KNO_3) was purchased from Acros Organics (New Jersey, USA). Phosphate buffer saline (PBS) was purchased from Mediatech, Inc. (Manassas, USA).

A power supply was purchased from Guangzhou Yihua Electronic Equipment Co., Ltd (China). A commercial bath sonicator (42 kHz) was purchased from Chicago Electric (Carol Stream, IL). Electric relays were purchased from Ningbo Songle Relay Co., Ltd (China). An Arduino Uno microcontroller was purchased from Spark Fun Electronics (Niwot, CO).

Sonoelectrodeposition system

The pulSED system consisted of a DC potential source (power supply) combined with a bath sonicator. To control the duty cycle (on/off timing and duration of the power supply and the sonicator), both components were outfitted with a relay that was controlled by an Arduino Uno microcontroller (see ESI Fig. S2†). A custom MatLab program was used to specify duty cycle parameters, (plating time, sonication time) and cycle numbers for all experiments (contact corresponding author to request Arduino code).

Four different plating schemes were compared in this study: (1) simultaneous sonoelectrodeposition (SED), in which neither the ultrasonic or plating potential were pulsed; (2) pulsed electrodeposition (PED), where the plating potential is pulsed, but no sonication is applied; (3) PED with constant sonication (SPED), where the plating potential is pulsed and the ultrasonic stimulus is not pulsed; and (4) pulsed sonoelectrodeposition (pulSED), in which the ultrasonic and plating potentials are pulsed out of phase. The parameters used to calculate duty cycle were the plating pulse time (T_{ON}), the ultrasonic pulse time (T_{US}) and the total number of pulse cycles (N_{CYCLE}). A visual schematic of these deposition treatments can be seen in ESI Fig. S3.† In the treatments that required pulsing, the plating pulse time (T_{ON}) and sonication pulse time (T_{US}) were each 1 s, and the frequency of the duty cycle was varied as noted. As a control, platinum was also deposited with no pulsing of potential or sonication.

Nanoplatinum electrodeposition

Prior to nanomaterial deposition, the Pt/Ir electrodes were cleaned using 3 μm and subsequently 1 μm diamond suspensions, rinsed with methanol, and finally polished using an alumina slurry (0.05 μm). For all experiments fresh plating solutions were prepared with 0.72% chloroplatinic acid and 0.001% lead acetate in DI water at 20 °C. A polyethylene terephthalate cup (0.23 mm thick) containing a 20 mL aliquot of the plating solution was placed in the sonicator bath and the bath was filled with DI water. To minimize dissipation of the ultrasonic wave, the surface meniscus of the external water bath depth and the plating solution in the polyethylene terephthalate cup were maintained at the same height. In preliminary studies, the acoustic wave was measured to have a frequency of 29 kHz within the polyethylene cup. For electrodeposition, the Pt/Ir electrode and a platinum wire were connected to the cathode and anode of the power supply, respectively; and then immersed into the plating solution. A constant overpotential of 10 V (25 mA) was used for all electrodeposition during the plating cycle.

Electrode functionalization

For enzymatic glucose biosensors, a base layer of Nafion was formed on the nanoplatinum following the procedures in our previous manuscripts,[48,50,51] and an enzyme layer of glucose oxidase (GOx) and chitosan was then deposited. For glucose deposition, a solution was prepared by combining 5 mg of GOx per 50 μL of 1× PBS, and the solution was mixed at a 1 : 1 ratio with 0.05% chitosan solution. Then, a 2 μL aliquot of the enzyme–chitosan solution was drop cast onto the electrode and allowed to dry for 5 minutes at room temperature before testing.[49]

Electrochemical analysis

Electroactive surface area (ESA) was determined using cyclic voltammetry (CV) in ferrocyanide. CVs were performed with a 3 electrode electrochemical cell stand using a Ag/AgCl reference electrode and a platinum reference electrode at room temperature and pH 7.1. The CVs were conducted with a quiet time of 10 s, a switching potential of 650 mV and scan rates of 50, 100, 150, and 200 mV s^{-1} with 4 mM $Fe(CN)_6^{3-}$/1 M KNO_3. The ESA of each electrode was calculated using the Randles–Sevcik equation:

$$i_p = 2.69 \times 10^3 \cdot n^{\frac{3}{2}} \cdot A \cdot D^{\frac{1}{2}} \cdot C \cdot \nu^{\frac{1}{2}} \quad (1)$$

where: i_p is the reduction peak (A), n is the number of transferred electrons from the redox couple (n = 1), A is the electroactive surface area (cm^2), D is the diffusion coefficient (6.7×10^{-6} cm^2 s^{-1}), C is the concentration of the working solution (4 mol cm^{-3}), and $\nu^{1/2}$ is the scan rate (V s^{-1}).

DC potential amperometry (DCPA) was conducted using a BASi cell stand with PBS (pH = 7.1) at a working potential of +250 mV *vs.* a Ag/AgCl reference electrode for the non-enzymatic glucose biosensor, or +500 mV for the hydrogen peroxide and enzymatic glucose biosensors. Working electrodes were polarized for at least 30 minutes before successive additions of the appropriate analyte into the electrochemical cell. Sensitivity was determined by calculating the slope of the linear region of calibration curves, and the lower limit of detection (LOD) was calculated using the 3σ method. Response times (t_{95}) were calculated using the method described in Vanegas *et al.*[8] Selectivity was calculated in the presence of organic acids such as ascorbic acid (AA ≈ 0.1 mM), 4-aceaminophen (AP ≈ 0.1 mM) uric acid (UA ≈ 0.02 mM), which are commonly found in biological samples.

Imaging and material analysis

Scanning electron microscopy (JEOL 5600 LV, JEOL Ltd, Akishima, Japan) and scanning white light intereferometery (Zygo Newview 7200, Zygo Corporation, Middlefield, CT) were used to determine nanometal morphology and surface roughness, respectively using the methods in Vanegas *et al.*[8] and Burrs *et al.*[49] A solid state energy dispersive X-ray spectroscopy (EDS) detector (20kX) on a SEM 6400 was used for elemental analysis. The SEM images were taken at a magnification of 100 kX and with an acceleration voltage of 10.0 kV or 15.0 kV.

Particle size analysis was conducted using the particle analyzer function in Image J.

Statistical analysis

All measurements were conducted in triplicate and analyzed using ANOVA to test for significance. Individual effects were determined using a Bonferroni multiple comparison test.

Results and discussion

Comparison of various electrodeposition methods

In order to determine the effect of duty cycle and also tease out the contribution of pulsing *versus* sonication on ESA of nanoplatinum modified electrodes, four different treatments were tested: (i) sonochemical electrodeposition (SED), (ii) a combination of sonochemical and pulsed deposition that is not pulsed out of phase with (SPED), (iii) pulsed electrodeposition (PED), and (iv) biphasic pulsed sonication and electrodeposition (pulSED). As a control all treatments were compared to a bare Pt/Ir electrode and an electrode that was plated (potentiostatic) with magnetic stirring for agitation at a constant overpotential of 10 V.

Representative SEM images for each of the four treatments are shown in Fig. 1. Each of the four treatments produced dendritic-like platinum nanostructures, with some subtle differences in morphology and nanoparticle size. All platinum nanostructures in this work contained large base structures (600 to 900 nm in diameter; see ESI Fig. S4† for lower magnification images) that were decorated with smaller nanostructures, most of which were self-similar and fractal. All of the nanoplatinum consisted of fractal structures that resemble the influorescent region of romanesco broccoli and other similar members of the *Brassica* genus, which is similar to the hierarchical nanostructures developed by Liu *et al.*[27] The average size of surface features for SED and SPED nanostructures was 45.28 ± 1.7 nm and 33.67 ± 1.3 nm, respectively. The pulSED treatment formed the smallest surface features (26.31 ± 1.3 nm) and consisted of dendritic fractal structures as small as 5 nm. Similar Romanesco-like morphologies have been developed with other metals, including gold,[52,53] copper,[54] zinc oxide,[55] cadmium sulfide,[56] and indium tin oxide.[54] Nanoplatinum formed by PED (Fig. 1c) had an average nanoparticle size of 46.54 ± 1.9 nm, with unique features among the four treatments that were similar to nanocorals. Nanocoral morphologies with this characteristic morphology have been synthesized with gold[57] and platinum.[8] These fractal patterns are known to maximize transport in natural and synthetic systems, which is of great importance in sensing applications.

The mean nanoparticle size for each of the four treatments was significantly different based on ANOVA ($p < 0.05$; $\alpha = 0.05$). A multiple comparison test (Bonferroni) indicated that nanoparticle size for SPED and pulSED treatments was significantly lower than PED and SED. The pulSED treatment had the lowest individual particle sizes relative to the other treatments and Fig. 1d shows that the distribution of the nanoparticles was in smaller aggregate structures, relative to the other treatments. Additionally, the pulSED and SPED treatments produced nanostructures with lower variability than the other two treatments. Although the SPED technique produced relatively homogenous fractal nanostructures, the SEM images indicate a higher degree of aggregation, which is likely the source of the relatively high mean nanoparticle diameter. Other studies

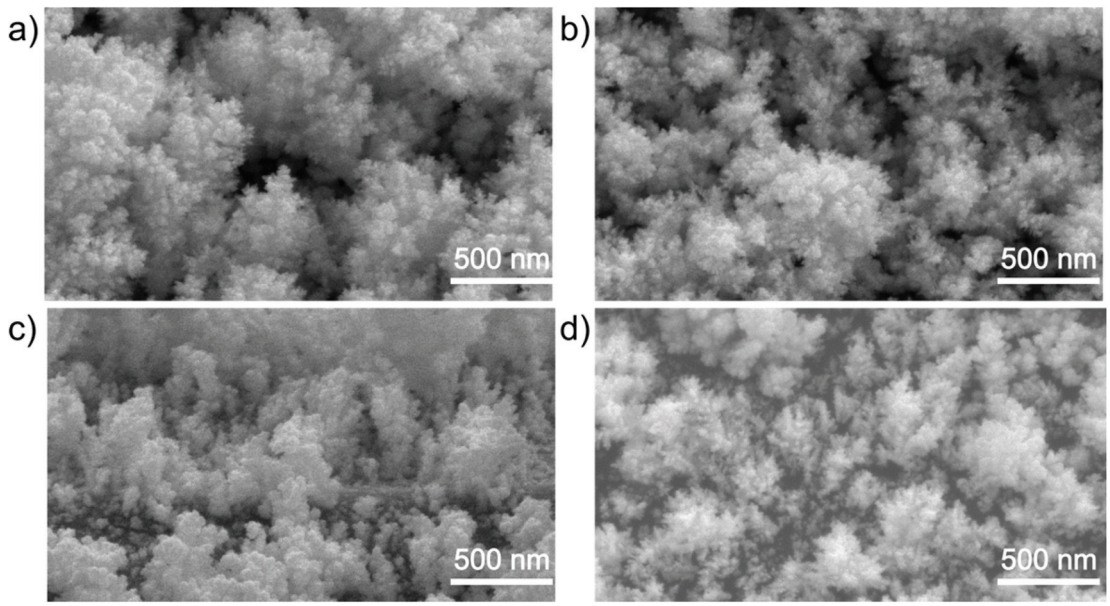

Fig. 1 Scanning electron micrographs for various treatments (a) SED (45.28 ± 1.7 nm), (b) SPED (33.67 ± 1.3 nm), (c) PED (46.54 ± 1.9 nm), (d) pulSED (26.31 ± 1.3 nm). The individual deposited surface particles were significantly smaller for the pulSED and the SPED treatment, though the SPED particles aggregated into larger structures compared to pulSED.

using PED have shown nanoparticle sizes near 70 nm, and studies using SED have produced nanoparticles as large as 960 nm.[38,58] For pulSED fractal nanoplatinum, the significant reduction in nanoparticle size is likely due to enhanced migration of dissolved metal ions to the electrode surface during the relaxation phase due to cavitation caused by the ultrasound wave. This cavitation deters formation of structures that aggregate into amorphous or unstable nanostructures.

EDS data (see ESI Table S1† for details) indicate that the fractal structures observed in Fig. 1 had various amounts of oxygen, platinum, and lead surface groups. In general, pulSED and PED treatments formed more stable structures that promote oxidation of glucose or hydrogen peroxide, with the pulSED treatment forming the most efficient structure (discussed in Fig. 3–6). Surface oxygen content was higher for SED and SPED treatments relative to the PED and pulSED deposition, which is likely platinum oxide. Guo *et al.*[83] found that electrodeposition of platinum onto carbon nanotubes first results in formation of platinum oxide (specifically octahedral Pt(IV) complexes), followed by formation of stable platinum nanoparticles; the platinum oxide complexes are thus a precursor of nanoplatinum. Thus, the PED and pulSED treatments contained more nanoplatinum than platinum oxide groups relative to the SED and SPED treatments based on EDS. Platinum oxide is known to oxidize glucose at overpotential greater than 1.0 V, although this was not studied in detail here since the selectivity of platinum oxide over organic acids is poor.[37] The surface-bound Pb was at least 8 times higher for the pulSED treatment than SED and SPED, and twice as high as the PED treatment. For non-enzymatic glucose sensing, this is important since Pt–Pb nanostructures are known to improve selectivity over interfering species such as AA, UA, and AP by lowering the overpotential for glucose oxidation. Both Pt_M (edge energy = 3.3 keV) and PtL_α (edge energy = 9.4 keV) peaks were detected for each of the four treatments (see ESI Fig. S5 and S6† for details). Only a small fraction of L band electrons were destabilized relative to M band electrons, indicating the metal nanostructures were stable up to the X-ray emission depth (which is approximately 1–2 μm). Based on EDS, the SED and SPED techniques did not form stable nanoplatinum structures as quickly/efficiently as the PED/pulSED treatments (deposition time was the same for all treatments). As discussed below, the results are validated by cyclic volammetry and DC potential amperometry (Fig. 2). The pulSED method uses considerably less platinum in the overall structure compared to the other techniques and forms more stable nanoplatinum structures. Nanoplatinum formed using SPED and PED contained significantly higher levels of platinum metal (approximately 10–20% more metal on a percent weight basis and a percent atomic mass basis than pulSED). This is an important finding since the cost of platinum has more than tripled since 2010.

Cyclic voltammetry and oxidative amperometry

All CVs showed reversible redox behavior for each treatment in ferrocyanide solutions (representative CVs shown in Fig. 2a). Peak oxidative and reductive current for the pulSED treatment was significantly higher ($p < 0.0001$, $\alpha = 0.05$) than all the other treatments, followed by PED, SED, and SPED in order of decreasing peak potential. Fig. 2b shows the average ESA for each of the electrode treatments, which followed the same trend as the representative CV in Fig. 2a. The ESA for all four treatments in Fig. 2 were significantly higher than a bare Pt/Ir electrode (0.016 ± 0.001 cm^2) and an electrode platinized at 10 V with magnetic stirring for the same plating time (0.032 ± 0.001 cm^2). This trend was expected, as traditional galvanostatic and potentiostatic electrochemical plating is subject to diffusion limitations and formation of gaseous hydrogen byproducts at the deposition site.[59,60] The formation of hydrogen bubbles on the electrode significantly reduces the accessible surface sites for nucleation of metal ions and diminishes the effect of applying a higher overpotential.[31] Among the various treatments, the average ESA for pulSED (0.28 ± 0.04 cm^2) and PED (0.27 ± 0.03 cm^2) was significantly

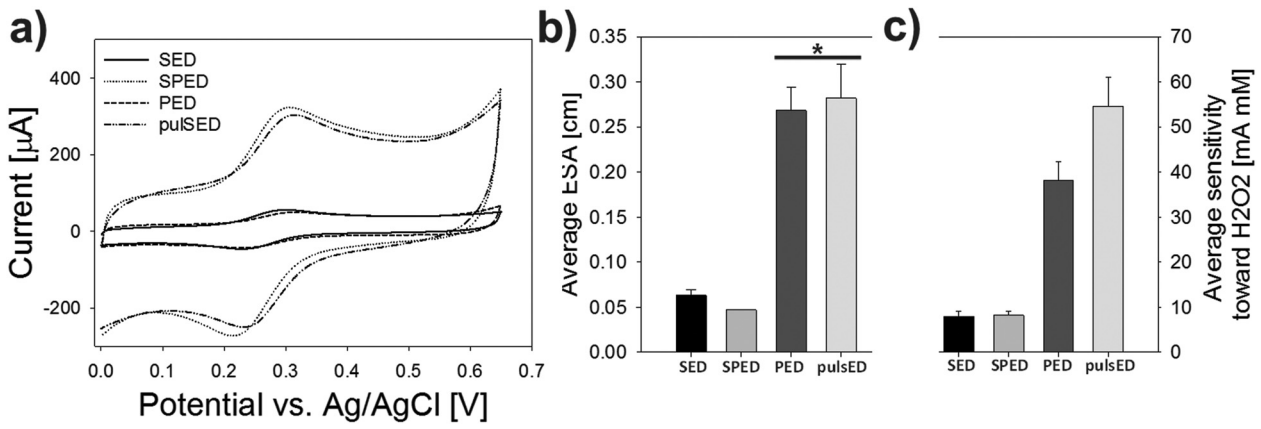

Fig. 2 (a) Representative cyclic voltammograms for the four treatments (scan rate = 200 mV s^{-1}). (b) Average electroactive surface area for all plating treatments. The single asterisk (*) indicates treatments that were significantly higher ($p < 0.05$) than the other treatments. The error bars denote the standard error ($n = 3$). (c) Average sensitivity toward H_2O_2 for all plating treatments. In the treatments that required pulsing for panels b and c, the plating pulse and sonication pulse were each 1 s in length. The duty cycle was 500 mHz and all treatments had a total plating time of 90 s.

higher than SED (0.06 ± 0.01) and SPED (0.05 ± 0.01 cm^2) (p = 0.01, α = 0.05; one way ANOVA). Sensitivity towards H_2O_2 was assessed for each electrode treatment to directly compare the Faradaic current under oxidative potential (Fig. 2c). The trends for peroxide sensitivity were nearly identical to those observed for electroactive surface area (see ESI Fig. S7†), with one key difference: the nanoplatinum formed using the pulSED technique had a significantly higher sensitivity (54.6 ± 6.4 μA mM^{-1}) than all the other treatments ($p < 0.001$, $\alpha = 0.05$).

Together, these results indicate that the primary contributing parameter to enhancing ESA is the pulsing of applied potential, but that continuous sonication destabilized formation of nanometal on the electrode surface. Although there was no significant difference in ESA for pulSED *versus* PED at 500 mHz and a total plating time of 90 s, there was a significant increase in H_2O_2 sensitivity and a change in metal morphology/particle size. As discussed in Fig. 4 and the related section, increasing the pulSED duty cycle to 990 mHz increased ESA by an additional 30%, and resulted in an additional improvement in sensing performance. To further explore the effect of sonication on the deposition of nanoplatinum, an additional one-way ANOVA (α = 0.05) was performed only considering the SED and SPED treatments. Surprisingly, SED (constant sonication and electrodeposition) had a significantly higher ESA than SPED ($p < 0.05$), lower surface oxygen content, and higher platinum content. This was not expected since previous studies have indicated that use of SED (*i.e.*, the presence of a continuous ultrasonic wave) results in formation of amorphous platinum clusters, leading to the formation of loosely packed (unstable) aggregate structures with relatively low ESA.[41,61,62] Since the SPED treatment used a pulsed potential, we expected this treatment to produce a higher average ESA than SED. We presume that the underlying mechanism for this finding is the destabilization of nanostructures by the ultrasound wave, which then caused detachment and formation of amorphous clusters in suspension during the relaxation phase.

Fig. 3 shows the relationship between average nanoparticle size and ESA for this work and similar nanoplatinum structures in the recent literature. All of the materials in Fig. 3 were prepared by electrodeposition of nanoplatinum onto platinum electrodes. An empirical (non-deterministic) exponential model (solid line) with a 3SD confidence interval (dashed line) is shown. As expected, there is an exponential relationship between deposited nanoparticle size and ESA for electrodes prepared using similar techniques. Other researchers predict a similar trend using deterministic models describing conductivity of nanosilver,[63] nanoalumina,[64] nanogold,[65] fractal nanofilms[66] and nanosilica.[67] For the data in Fig. 3, the highest previously reported ESA was reported by Vanegas *et al.*, where average nPt size was 4 ± 1 nm for a homogenous "graphene sandwich" structure.[8] Chaturvedi *et al.*[48] used pulSED (500 mHz) to deposit homogenous nanoplatinum films on nanoceria modified electrodes to promote dismutase reactions in detection of purines (average nPt size was 60 ± 10 nm). The average ESA for the nanoceria hybrid material was relatively low (0.06 ± .01 cm^2), although this was due to inclusion of nanoceria in the film as discussed in detail.[48] Burrs *et al.* used pulSED deposition at 500 mHz to deposit nanoplatinum on reduced graphene oxide (average ESA was 0.21 ± 0.02 cm^2), although the data is not included in Fig. 3 since no SEM micrographs were published with this work.[49] Shi *et al.* used standard ED to form amorphous nanoplatinum islands and aggregate structures with an average particle size ranging from 250 to 600 nm, and an ESA of approximately 0.04 cm^2.[68,69]

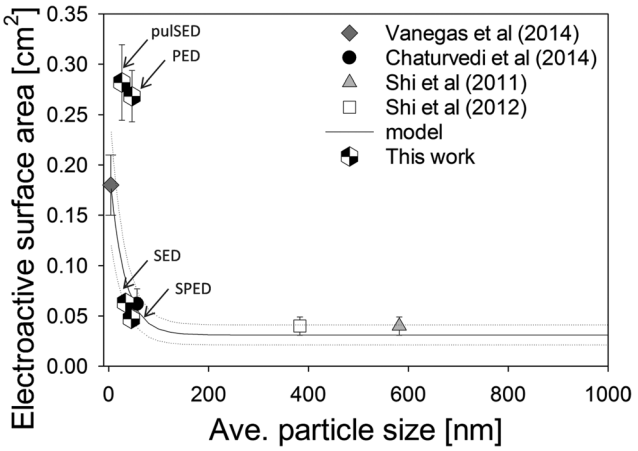

Fig. 3 Electroactive surface area as a function of nanoplatinum size. As expected, smaller nanoparticles significantly increase electroactive surface area. PED and pulSED nanoplatinum were five to six times higher than expected based on previous work with nPt electrodeposition (noted on the graph). An empirical (non-deterministic) model is represented by the solid line, and the confidence interval at 3SD is shown as a dotted line for the upper and lower bounds. ESA for SED and SPED treatments can be approximated by the model, but the PED and pulSED nanoplatinum were five to six times higher than predicted by the model.

The ESA of the SED and SPED nanoplatinum were within the expected range based on the empirical model developed with previously published work on similar nanoplatinum. However, the PED and pulSED nanoplatinum were five to six times higher than expected.

The pulSED current density in this work was relatively low (0.5 mA cm^{-2}), which is well below the upper limit for PED; in previous studies the ESA did not increase when current density was higher than 200 mA cm^{-2} due to the evolution of hydrogen gas at the surface of the electrode.[70,71] The data in Fig. 2 and 3 indicate that the pulsing effect is the main parameter for enhancing ESA for nanoplatinum-modified electrodes.

Based on particle size analysis, ESA, and peroxide sensitivity, use of pulSED or PED results in formation of fractal nanometal structures with relatively small/homogenous nanoparticles, excellent ESA, and high sensitivity to peroxide due to collapse of bubbles during the relaxation phase by acoustic cavitation. As shown in the following section, changing the duty cycle and total plating time can improve nanometal deposition for the pulSED treatments relative to PED.

Effect total plating time and duty cycle on pulSED nanometal

The effect of total plating time on ESA was first studied at a constant pulSED duty cycle of 500 mHz while varying the number of total cycles. Fig. 4a shows that as total plating time is increased the ESA also increases, as expected. Increasing total plating time results in the deposition of more metal onto the electrode (see ESI eqn (S1) and (S2)†). To test the upper limits of the pulSED technique in terms of plating time, platinum was deposited at 500 mHz with a total plating time of 720 s. The ESA (3.64 ± 0.78 cm^2), was 10 times higher than all conditions shown in Fig. 4a, but the platinum was not reliable for fabricating biosensors because the deposited metal extended beyond the geometrical surface of the electrode (overgrowth) and was not stable; the material flaked off when immersed in solution. Thus, the data for a pulSED plating time of 720 s is not discussed in detail.

The effect of duty cycle on pulSED nanometal (total plating time of 20 s and relaxation time of 1 s for each experiment) is shown in Fig. 4b. As duty cycle increases from 166 mHz (average ESA was 0.034 ± 0.015 cm^2) to 500 mHz (ESA was 0.048 ± 0.008 cm^2), there is an increase in ESA of approximately 30% (also see ESI Fig. S8† for CVs). Further increasing the duty cycle to 667 mHz increased the ESA by an additional 80% (ESA was 0.282 ± 0.038 cm^2). A duty cycle of 990 mHz (ESA was 0.40 ± 0.09 cm^2) resulted in an order of magnitude improvement in ESA when compared to 166 mHz, and two orders of magnitude higher than bare Pt/Ir. We attribute this effect to mixing of the dissolved metal ions within the boundary layer at the sensor surface due to microjetting of gas bubbles and convection of ions within the double layer. For low duty cycles, there is longer deposition time and thus the process depletes more metal ions and is subject to diffusion limitations. This result shows similar trends as what has been shown for galvanostatic PED[70] and potentiostatic PED,[71] where the duty cycle also strongly influences ESA. Low duty cycle causes diffusion limitations that hinder metal deposition; too high of a duty cycle leads to current limitations at the electrode surface and less dendritic growth. It should be noted that the trends observed here are somewhat different than those involving SPED for the production of suspended particles at lower sonication frequencies. In suspensions, others have shown that high duty cycle produces fewer nucleation sites available for nanometal formation.[42,72] In suspension, metal ions are destabilized and disperse from the nanoparticle *via* acoustic wave action before they can bond and form nanoparticles.

To study the trends observed in Fig. 4 related to nanoplatinum morphology, scanning white light interferometry (SWLI) was used to characterize the surface roughness over the entire electrode surface area. Representative SWLI images for various duty cycles are shown in Fig. 5a–c. As expected, surface roughness increases with increasing duty cycle, and the highest RMS surface roughness (2236 nm) was measured for a duty cycle of 990 mHz (see ESI Fig. S9† for details). Even at the lowest duty cycle tested (500 mHz), the surface roughness (286 nm) was a six-fold improvement over previously reported RMS values using SED (51 nm).[62] The SWLI images below, on the other hand, are an area of approximately 4×10^{-2} mm^2, which is the approximate size of the Pt/Ir electrode.

Amperometric sensors based on pulSED nanoplatinum

To demonstrate the utility of the technique for fabrication of highly efficient electrochemical sensors, pulSED nanoplatinum was used as a transducer platform for development of non-enzymatic and enzymatic sensors for detecting hydrogen peroxide or glucose. A duty cycle of 990 mHz was used to deposit nanoplatinum onto a Pt/Ir electrode for all sensors.

For the non-enzymatic glucose sensor, characteristic CVs (see ESI Fig. S10†) show anodic and cathodic peaks at −0.38 V, −0.1 V, and +0.25 V. The anodic peak at −0.38 V is attributed to the adsorption of intermediate byproducts, while the anodic peak beginning at +0.25 V and the cathodic peak at −0.1 V are the direct oxidation of glucose as other studies have also shown.[73,74]

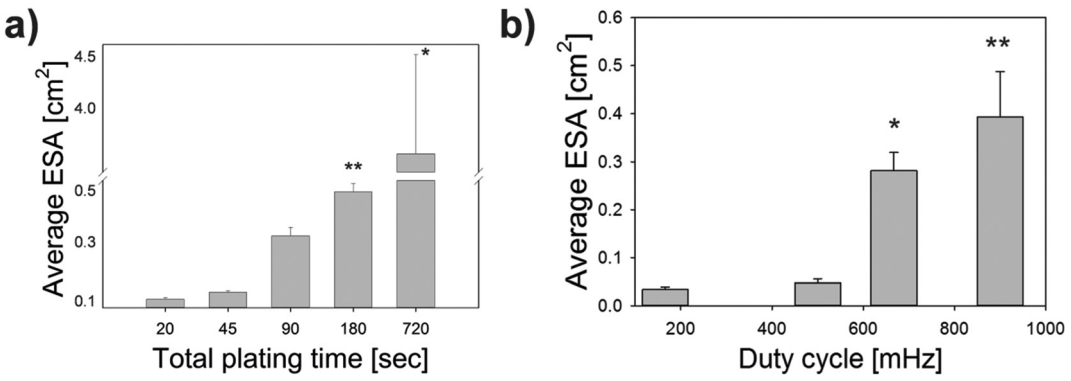

Fig. 4 (a) Effect of total plating time on electroactive surface area at a constant duty cycle of 500 mHz for pulSED. (b) Effect of duty cycle on the average electroactive surface area. The single asterisk (*) indicates treatments that were significantly higher ($p < 0.05$) than the other treatment with no asterisk, the double asterisk (**) indicates treatments that were significantly higher ($p < 0.05$) than all other treatments. The error bars denote the standard error ($n = 3$).

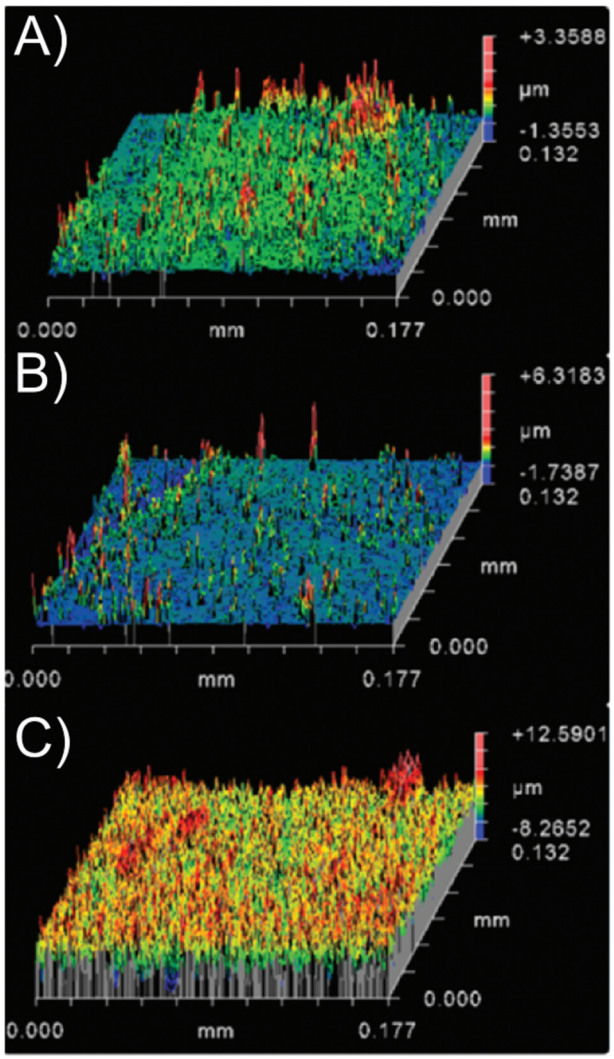

Fig. 5 Scanning white light interferometry (SWLI) images for pulSED nanoplatinum formed at various duty cycles. (a) 500 mHz (RMS = 286 nm), (b) 667 mHz (RMS = 1425 nm), and (c) 990 mHz (RMS = 2236 nm). RMS surface roughness increases with increasing duty cycle for all conditions tested.

Representative DCPA time series plots for non-enzymatic detection of hydrogen peroxide (Fig. 6a) and glucose (Fig. 6b) indicate a classic steady state response after addition of the target analyte (vertical arrows indicate injection of target analyte). The characteristic spikes seen in panels a and b after injection of analyte are due to diffusion of analyte to the surface followed by oxidation of target species.[75] DCPA for enzymatic detection of glucose (Fig. 6c) did not contain these "spikes" in oxidative current after injection of analyte, which is due to diffusion of target analyte through the enzyme membrane prior to transport of Faradaic current. Calibration plots for each sensor (Fig. 6d) show that all sensors exhibited a linear response within a concentration range of 40 µM to 1 mM (R^2 > 0.99). The LOD varied for each sensor from 4 to 40 µM and the sensitivity also varied as discussed in Table 1. The GOx biosensor sensitivity decreased significantly above concentrations of 2 mM due to enzyme saturation and diffusion limitations (the enzyme was encapsulated in a chitosan membrane), while the non-enzymatic sensors were linear up to 6 mM. Sensitivity towards peroxide was twice as high for concentrations below 1 mM, which has been shown in similar work for low overpotential. For all sensors, the response time was from 1–2 s within the linear range (see ESI Fig. S11† for details).

The performance characteristics of the three sensors in Fig. 6 relative to other devices in the current literature are shown in Table 1. Overall, the pulSED nanoplatinum transducer layer in this work had the high sensitivity to hydrogen peroxide compared to similar electrodes. This high sensitivity is attributed to the fact that the normalized ESA of the pulSED modified electrode is approximately 14 times larger than an unmodified electrode, which allows for more effective charge transfer following the degradation of peroxide. The underlying mechanism of this increased electroactivity is the morphology of the fractal metals, which is an optical transport network based on minimization of energy required for system fluxes. The LOD for peroxide (7.1 ± 6.9 µM) was slightly higher than most of the reported peroxide sensors in literature. While Chakraborty and Raj[76] report an extremely low LOD for their peroxide sensor, there is no reported error and the reproducibility is not known.[76] The average t_{95} for peroxide sensing was 1.7 ± 0.4 s, which was faster than previously reported values using similar nanomaterials. While sensors such as the nanomaterial hybrids are higher than we report here (see Chen *et al.*[77] for review), our method is a one pot, single material electrode which does not require any expensive/complicated instrumentation and is competitive with more cumbersome deposition techniques/hybrid materials when accounting for the batch to batch error.

Non-enzymatic detection of glucose at +0.25 V was studied at pH 7.1 in PBS. The sensitivity (73 ± 14 µA cm^{-2} mM^{-1}) is comparable to other platinum electrodes, and higher than all sensors to date that used the same overpotential. The Pt–Ni nanotubes by Sun *et al.*[73] had a higher sensitivity, but the overpotential was significantly higher (+350 mV). The LOD for non-enzymatic glucose detection is comparable to other electrodes in the recent literature (when accounting for sensor-to-sensor variability), and the average response time is better than other sensors published to date. Although hysteresis was not tested in this study, sensor poisoning by intermediates of glucose oxidation and chloride ions is a known problem for non-enzymatic platinum electrodes and should be considered.[37]

To our surprise, the pulSED nanoplatinum biosensor (with GOx) had a higher average sensitivity than most recent devices based on nanocarbon,[68] and nanoceria/nanocarbon,[48] despite being composed solely of nanoplatinum. The LOD of the glucose sensor (3.8 ± 1.2 µM) was lower than most other reported values for nano-carbon-metal composites as shown in Table 1. The t_{95} of the glucose biosensor was 2.0 ± 0.6 s, which is slightly faster than the other reported sensors, though a number of studies using similar materials did not report a t_{95}.

The selectivity of each glucose sensor over AA (0.1 mM), UA (0.05 mM), and AP (0.1 mM) was analyzed in PBS (see ESI

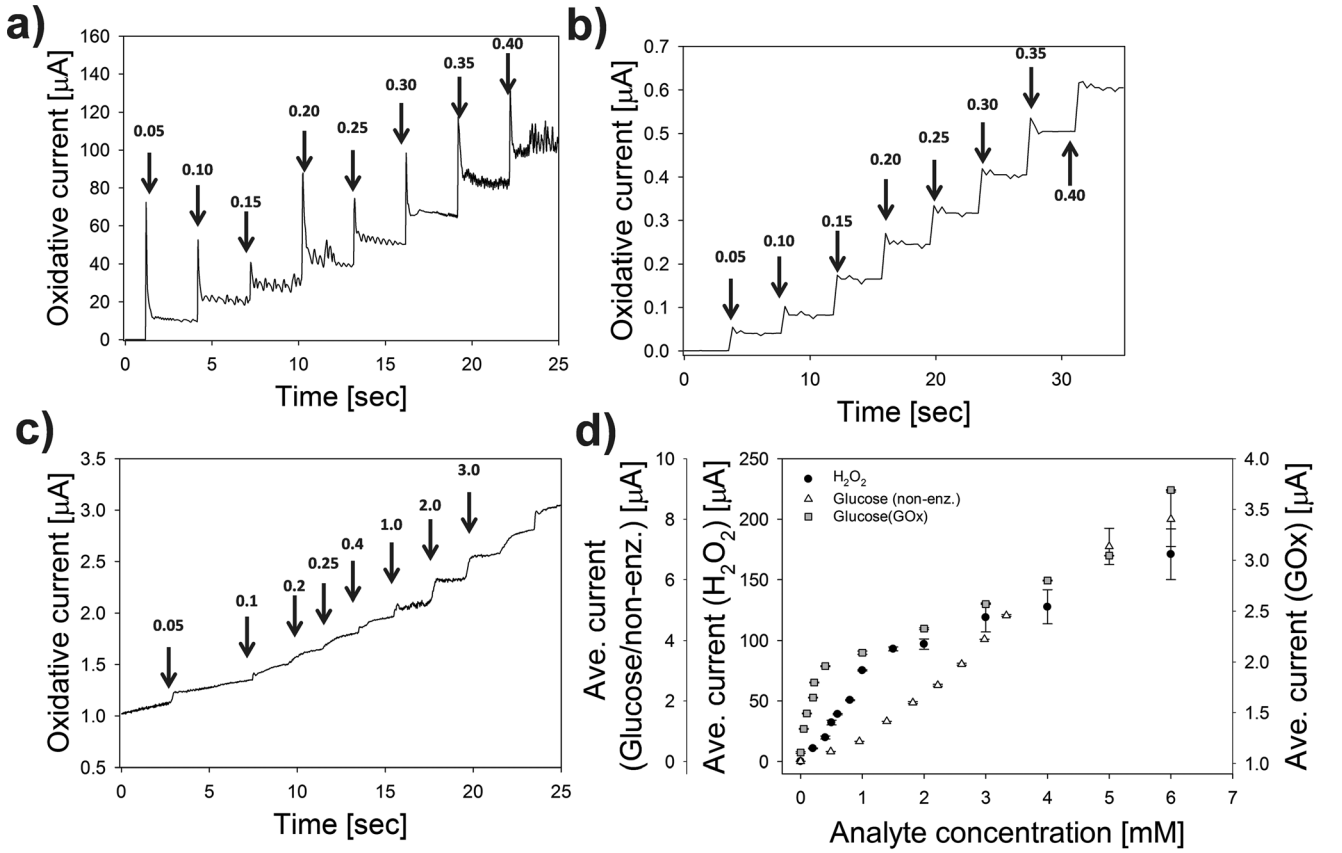

Fig. 6 Performance of hydrogen peroxide and glucose sensors based on pulSED nanoplatinum as a transducer layer. Non-enzymatic sensing of (a) hydrogen peroxide at +500 mV in PBS at pH 7.4, or (b) glucose at +250 mV in PBS at pH 7.1. (c) Enzymatic sensing of glucose at +500 mV in PBS at pH 7.4. The vertical arrows in panel c indicates time points when analyte was added to the electrochemical cell. (d) Average calibration plots for all three sensors shown in panels a–c (n = 3 electrodes, error bars denote standard error).

Table 1 Comparison of performance characteristics for recent hydrogen peroxide and glucose sensors

Sensor	Platform	Sensitivity [μA cm^2 mM^{-1}]	Detection limit [μM]	Response time [s]	Ref.
Non-enzymatic hydrogen peroxide sensing	pulSED nPt	3335 ± 305	7.1 ± 6.9	1.65 ± 0.42	This work
	Pt/Ir-MWCNT-nPt	2450 ± 750	0.43 ± 32	3 ± 22	Vanegas *et al.*[8]
	Pt/Ir-nPt-GO-nPt	2250 ± 350	0.14 ± 28	3 ± 14	Vanegas *et al.*[8]
	Pt hierarchical nanoflowers	1150 ± NR	1.05 ± NR	NR	Heli *et al.*[62]
	nPt-RGO-nCe-nPt	555 ± 190	0.5 ± 0.3	NR	Chaturvedi *et al.*[48]
	Nano-Pt	460 ± NR	5×10^{-4} ± NR	NR	Chakraborty & Raj[76]
	Mesoporous Pt	140 ± NR	4.5 ± NR	NR	Evans *et al.*[81]
Non-Enzymatic glucose sensing	pulSED nPt (+250 mV)	72.9 ± 13.8 (pH = 7.1)	65 ± 28	1.6 ± 0.5	This work
	Pt–Ni nanotubes (−350 mV)	124.2 ± NR (pH = 7.0)	32 ± NR	3.5 ± NR	Sun *et al.*[73]
	nPt on gold coated wafer (+400 mV)	66.5 ± NR (pH = xx)	40 ± NR	NR	Roh & Kim[80]
	nPt clusters on graphene (+500 mV)	1.21 ± NR (pH = 7.4)	30 ± NR	3 ± NR	Chang *et al.*[78]
	Pt–Pd nanocubes on graphene (+250 mV)	1.4 ± NR (pH = 7.4)	NR	NR	Chen *et al.*[77]
Enzymatic glucose biosensing	pulSED nPt/chitosan-Gox	155 ± 25	3.8 ± 1.2	2.03 ± 0.58	This work
	nPt/RGO/nCe/nPt/TEOS-Sol-Gox	65 ± 5	1.3 ± 0.6	6.3 ± 3.4	Chaturvedi *et al.*[48]
	TEOS/GOx	60 ± 15	2.0 ± NR	<8.0	Shi *et al.*[68]
	SWNT/nPt/GCE/GOx	105 ± NR	0.5 ± NR	NR	Hrapovic *et al.*[32]
	Au/MWNT/GOx	85 ± NR	10.0 ± NR	NR	Wang *et al.*[34]
	Au/nAu/Chitosan/Gox	5 ± NR	2.7 ± NR	NR	Luo *et al.*[82]

NR indicates values that were not reported.

Fig. S12†). For each sensor, the selectivity for 1 mM glucose over all interferents was ≥95%. For non-enzymatic sensing, Chang *et al.*[78] reported similar selectivity for a nPt-graphene modified electrode at pH 7.4 and Sun *et al.*[73] prepared Pt–Ni nanotubes with similar selectivity at pH 7.0. No percent selectivity was reported in these previous studies, thus selectivity data cannot be directly compared. The selectivity of the GOx biosensor was higher than the non-enzymatic sensor (≥99.2%) which is attributed to the inclusion of a Nafion layer at the electrode surface. Although GOx indeed possesses a higher affinity for glucose than the nanoplatinum, the innate selectivity is relatively poor because the sensor must be operated at a high overpotential (+500 mV). Thus, we attribute the selectivity over organic acids to the Nafion layer. Further studies are needed to compare GOx biosensors to non-enzymatic sensors regarding sensor poisoning by chloride ions and oxidation byproducts, as these are major limitations for non-enzymatic glucose sensors.

In future studies, the pulSED system can be combined with other semiconductor and nanomaterial platforms such as graphene oxide, multi-walled nanotubes, or nanoceria[6,7,79] to produce reliable hybrid materials with excellent conductivity for sensing. Although we did not use the technique to grow nPt on electrode arrays, we did repeat the pulSED procedure and test in triplicate, which provides insight into sensor-to-sensor variability as shown in Table 1. This work shows that the technique does have promise for electrodeposition of multiple electrodies such as in a biochip microarray. Furthermore, this study compares enzymatic and non-enzymatic glucose sensing on nanoplatinum and provides insight into the role of nanoplatinum morphology and size on the oxidation of target analyte.

Conclusion

A wide variety of deposition methods exist for the formation of nanostructures based on noble and non-noble metals, and these structures have been used as a transducer material for electrochemical sensing. This study investigated the benefits of combining two known deposition techniques, pulse electrodeposition and sonoelectrodeposition (*i.e.* pulsed sonoelectrodeposition or pulSED), and the parameters that are used to control duty cycle. We showed that a high duty cycle resulted in higher electroactive surface area, with key differences in fractal morphology (resembling Romanesco broccoli). This can be attributed to the stabilization of nanostructures due to the uniformity in deposition offered by pulsed electrodeposition together with the reduction of gaseous byproducts by sonication, resulting in increased mass transfer to the electrode surface. The technique facilitates enhanced control of nanometal particle size and uniformity for development of fractal structures without the addition of capping agents. For the first time, we demonstrate use of this facile method for synthesis of fractal nanoplatinum structures as the transducer layer in amperometric sensing for enzymatic and non-enzymatic electrodes. The simple one pot, single material technique is competitive with (or superior to) other nanoplatinum materials in the current literature.

Acknowledgements

The authors would like to thank the UF Agricultural and Biological Engineering Fellowship (MT), the Colombian funding agencies Colfuturo and Colciencias (DV; no. 001375882), the UF Excellence Award (EMC; USDA/NIFA Hatch Project no. FLAABE-005062), and the NASA Florida Space Grant Consortium (EM; grant no. 00091356) for funding.

References

1 N. Shipway, E. Katz and I. Willner, *Angew. Chem., Int. Ed.*, 2000, **39**, 19–52.
2 D. Vairavapandian, P. Vichchulada and M. D. Lay, *Anal. Chim. Acta*, 2008, **626**, 119–129.
3 A. Kloke, F. Von Stetten, R. Zengerle and S. Kerzenmacher, *Adv. Mater.*, 2011, **23**, 4976–5008.
4 A. Ambrosi, A. Merkoçi and A. de la Escosura-Muñiz, *TrAC, Trends Anal. Chem.*, 2008, **27**, 568–584.
5 A. Walcarius, S. D. Minteer, J. Wang, Y. Lin and A. Merkoçi, *J. Mater. Chem. B*, 2013, **1**, 4878.
6 J. C. Claussen, A. D. Franklin, A. U. Haque, D. Marshall Porterfield and T. S. Fisher, *ACS Nano*, 2009, **3**, 37–44.
7 J. C. Claussen, A. Kumar, D. B. Jaroch, M. H. Khawaja, A. B. Hibbard, D. M. Porterfield and T. S. Fisher, *Adv. Funct. Mater.*, 2012, **22**, 3399–3405.
8 D. C. Vanegas, M. Taguchi, P. Chaturvedi, S. Burrs, M. Tan, H. Yamaguchi and E. S. Mclamore, *Analyst*, 2014, **139**, 660–667.
9 T. Hezard, K. Fajerwerg, D. Evrard, V. Collière, P. Behra, P. Gros, V. Collire, P. Behra and P. Gros, *J. Electroanal. Chem.*, 2012, **664**, 46–52.
10 J. C. Claussen, M. M. Wickner, T. S. Fisher and D. M. Porterfield, *ACS Appl. Mater. Interfaces*, 2011, **3**, 1765–1770.
11 G. P. Jin, Y. F. Ding and P. P. Zheng, *J. Power Sources*, 2007, **166**, 80–86.
12 W.-C. Tsai, C.-C. Wan and Y.-Y. Wang, *J. Electrochem. Soc.*, 2003, **150**, C267.
13 B. J. Plowman, S. K. Bhargava and A. P. O'Mullane, *Analyst*, 2011, **136**, 5107.
14 E. S. McLamore, D. M. Porterfield and M. K. Banks, *Biotechnol. Bioeng.*, 2009, **102**, 791–799.
15 S. Shahrokhian, R. Salimian and S. Rastgar, *Mater. Sci. Eng., C*, 2014, **34**, 318–325.
16 C. Carraro, R. Maboudian and L. Magagnin, *Surf. Sci. Rep.*, 2007, **62**, 499–525.
17 K. Ariga, A. Vinu, Y. Yamauchi, Q. Ji and J. P. Hill, *Bull. Chem. Soc. Jpn.*, 2012, **85**, 1–32.

18 Y. D. Fernandez, L. Sun, T. Gschneidtner and K. Moth-Poulsen, *APL Mater.*, 2014, **2**, 010702.
19 J. R. Banavar, T. J. Cooke, A. Rinaldo and A. Maritan, *Proc. Natl. Acad. Sci. U. S. A.*, 2014, **111**, 3332–3337.
20 J. N. Zheng, L. L. He, C. Chen, A. J. Wang, K. F. Ma and J. J. Feng, *J. Power Sources*, 2014, **268**, 744–751.
21 C. Liu, F. Su, J. Liang and P. Huang, *Surf. Coat. Technol.*, 2014, **258**, 580–586.
22 J. C. Claussen, J. B. Hengenius, M. M. Wickner, T. S. Fisher, D. M. Umulis and D. M. Porterfield, *J. Phys. Chem. C*, 2011, **115**, 20896–20904.
23 J. C. Claussen, M. A. Daniele, J. Geder, M. Pruessner, A. J. Makinen, B. J. Melde, M. Twigg, J. M. Verbarg and I. L. Medintz, *ACS Appl. Mater. Interfaces*, 2014, **6**, 17837–17847.
24 K. M. Marr, B. Chen, E. J. Mootz, J. Geder, M. Pruessner, B. J. Melde, R. R. Vanfleet, I. L. Medintz, B. D. Iverson and J. C. Claussen, *ACS Nano*, 2015, **9**, 7791–7803.
25 J. Simonet, *J. Electroanal. Chem.*, 2006, **593**, 3–14.
26 I. Sriram, E. Alexandra, A. Curtin, A. Chiaramonti, J. Cuchiaro, A. Weidner, T. Tingley, L. Greenlee and K. Jeerage, *J. Nanopart. Res.*, 2015, **17**, 1–11.
27 J. Liu, W. Hu, C. Zhong and Y. F. Cheng, *J. Power Sources*, 2013, **223**, 165–174.
28 W. Li, Y. He, L. Wang, G. Ding, Z. Q. Zhang, R. W. Lortz, P. Sheng and N. Wang, *Phys. Rev. B: Condens. Matter Mater. Phys.*, 2011, **84**, 045431.
29 A. Gutes, I. Laboriante, C. Carraro and R. Maboudian, *Sens. Actuators, B*, 2010, **147**, 681–686.
30 E. J. Coleman and A. C. Co, *J. Catal.*, 2014, **316**, 191–200.
31 R. M. Penner, *J. Phys. Chem. B*, 2002, **106**, 3339–3353.
32 S. Hrapovic, Y. Liu, K. B. Male and J. H. T. Luong, *Anal. Chem.*, 2004, **76**, 1083–1088.
33 S. D. Thompson, L. R. Jordan and M. Forsyth, *Electrochim. Acta*, 2001, **46**, 1657–1663.
34 C. Wang, M. Waje, X. Wang, J. M. Tang, R. C. Haddon and Yan, *Nano Lett.*, 2004, **4**, 345–348.
35 W. Gao, S. Sattayasamitsathit, J. Orozco and J. Wang, *J. Am. Chem. Soc.*, 2011, **133**, 11862–11864.
36 S. Campuzano, J. Orozco, D. Kagan, M. Guix, W. Gao, S. Sattayasamitsathit, J. C. Claussen, A. Merkoçi and J. Wang, *Nano Lett.*, 2012, **12**, 396–401.
37 S. Park, H. Boo and T. D. Chung, *Anal. Chim. Acta*, 2006, **556**, 46–57.
38 X. Chen, N. Li, K. Eckhard, L. Stoica, W. Xia, J. Assmann, M. Muhler and W. Schuhmann, *Electrochem. Commun.*, 2007, **9**, 1348–1354.
39 M. S. Chandrasekar and M. Pushpavanam, *Electrochim. Acta*, 2008, **53**, 3313–3322.
40 H. Natter and R. Hempelmann, *Electrochim. Acta*, 2003, **49**, 51–61.
41 V. Sáez and T. J. Mason, *Molecules*, 2009, **14**, 4284–4299.
42 V. Zin, B. G. Pollet and M. Dabalà, *Electrochim. Acta*, 2009, **54**, 7201–7206.
43 I. Haas, S. Shanmugam and A. Gedanken, *J. Phys. Chem. B*, 2006, **110**, 16947–16952.
44 A. Aqil, H. Serwas, J. L. Delplancke, R. Jérôme, C. Jérôme and L. Canet, *Ultrason. Sonochem.*, 2008, **15**, 1055–1061.
45 Q. Shen, L. Jiang, J. Miao, W. Hou and J.-J. Zhu, *Chem. Commun.*, 2008, 1683–1685.
46 R. Ganesan, S. Shanmugam and A. Gedanken, *Synth. Met.*, 2008, **158**, 848–853.
47 J. González-García, M. D. Esclapez, P. Bonete, Y. V. Hernández, L. G. Garretón and V. Sáez, *Ultrasonics*, 2010, **50**, 318–322.
48 P. Chaturvedi, D. C. Vanegas, M. Taguchi, S. L. Burrs, P. Sharma and E. S. McLamore, *Biosens. Bioelectron.*, 2014, **58**, 179–185.
49 S. L. Burrs, D. C. Vanegas, M. Bhargava, N. Mechulan, P. Hendershot, H. Yamaguchi, C. Gomes and E. S. Mclamore, *Analyst*, 2015, **140**, 1466–1476.
50 D. C. Vanegas, G. Clark, A. E. Cannon, S. Roux, P. Chaturvedi and E. S. Mclamore, *Biosens. Bioelectron.*, 2015, **74**, 37–44.
51 E. S. McLamore, J. Shi, D. Jaroch, J. C. Claussen, A. Uchida, Y. Jiang, W. Zhang, S. S. Donkin, M. K. Banks, K. K. Buhman, D. Teegarden, J. L. Rickus and D. M. Porterfield, *Biosens. Bioelectron.*, 2011, **26**, 2237–2245.
52 S. Sattayasamitsathit, A. M. O'Mahony, X. Xiao, S. M. Brozik, C. M. Washburn, D. R. Wheeler, W. Gao, S. Minteer, J. Cha, D. B. Burckel, R. Polsky and J. Wang, *J. Mater. Chem.*, 2012, **22**, 11950–11956.
53 H.-C. Liu, C.-C. Tsai and G.-J. Wang, *Nanotechnology*, 2013, **24**, 215101.
54 C. Kong, S. Sun, J. Zhang, H. Zhao, X. Song and Z. Yang, *CrystEngComm*, 2012, **14**, 5737.
55 M. Izaki, M. Watanabe, H. Aritomo, I. Yamaguchi, S. Asahina, T. Shinagawa, M. Chigane, M. Inaba and A. Tasaka, *Cryst. Growth Des.*, 2008, **8**, 1418–1421.
56 K. C. Wilson, E. Manikandan, M. Basheer Ahamed and B. W. Mwakikunga, *J. Alloys Compd.*, 2014, **585**, 555–560.
57 M. Xu, W. Qi, L. Zhang, J. Lai, Aziz-ur-Rehman, S. Majeed and G. Xu, *Microchim. Acta*, 2014, **181**, 737–742.
58 M. Q. Guo, H. S. Hong, X. N. Tang, H. D. Fang and X. H. Xu, *Electrochim. Acta*, 2012, **63**, 1–8.
59 A. Milchev and T. Zapryanova, *Electrochim. Acta*, 2006, **51**, 4916–4921.
60 A. Milchev and T. Zapryanova, *Electrochim. Acta*, 2006, **51**, 2926–2933.
61 *The Chemistry of Nanomaterials*, ed. C. N. R. Rao, A. Müller and A. K. Cheetham, Wiley-VCH Verlag GmbH & Co. KGaA, Weinheim, FRG, 2004.
62 H. Heli, N. Sattarahmady, R. Dehdari Vais and A. R. Mehdizadeh, *Sens. Actuators, B*, 2014, **192**, 310–316.
63 P. Warrier and A. Teja, *Nanoscale Res. Lett.*, 2011, **6**, 247.
64 M. P. Beck, Y. Yuan, P. Warrier and A. S. Teja, *J. Nanoparticle Res.*, 2008, **11**, 1129–1136.
65 M. A. H. Khalafalla, A. Mesli, H. M. Widattallah, A. Sellai, S. Al-harthi, H. A. J. Al-Lawati and F. O. Suliman, *J. Nanoparticle Res.*, 2014, **16**, 2546.

66 N. Riefler and L. Mädler, *J. Nanoparticle Res.*, 2009, **12**, 853–863.
67 G. Chen, W. Yu, D. Singh, D. Cookson and J. Routbort, *J. Nanoparticle Res.*, 2008, **10**, 1109–1114.
68 J. Shi, T.-G. Cha, J. C. Claussen, A. R. Diggs, J. H. Choi and D. M. Porterfield, *Analyst*, 2011, **136**, 4916–4924.
69 J. Shi, H. Zhang, A. Snyder, M. xian Wang, J. Xie, D. Marshall Porterfield and L. A. Stanciu, *Biosens. Bioelectron.*, 2012, **38**, 314–320.
70 H. Kim, N. P. Subramanian and B. N. Popov, *J. Power Sources*, 2004, **138**, 14–24.
71 W. Tang, S. Jayaraman, T. F. Jaramillo, G. D. Stucky and E. W. McFarland, *J. Phys. Chem. C*, 2009, **113**, 5014–5024.
72 M. Dabalà, B. G. Pollet, V. Zin, E. Campadello and T. J. Mason, *J. Appl. Electrochem.*, 2007, **38**, 395–402.
73 Y. Sun, H. Yang, X. Yu, H. Menga and X. Xu, *RSC Adv.*, 2015, **5**, 70387.
74 S. Cherevko and C. H. Chung, *Sens. Actuators, B*, 2009, **142**, 216–223.
75 E. S. McLamore, A. Diggs, P. Calvo Marzal, J. Shi, J. J. Blakeslee, W. A. Peer, A. S. Murphy and D. M. Porterfield, *Plant J.*, 2010, **63**, 1004–1016.
76 S. Chakraborty and C. Retna Raj, *Biosens. Bioelectron.*, 2009, **24**, 3264–3268.
77 W. Chen, S. Cai, Q.-Q. Ren, W. Wen and Y.-D. Zhao, *Analyst*, 2012, **137**, 49.
78 G. Chang, H. Shu, Q. Huang, M. Oyama, K. Ji, X. Liu and Y. He, *Electrochim. Acta*, 2015, **157**, 149–157.
79 J. C. Claussen, M. S. Artiles, E. S. Mclamore, S. Mohanty, J. Shi, J. L. Rickus, T. S. Fisher and D. M. Porterfield, *J. Mater. Chem.*, 2011, **21**, 11224–11231.
80 S. Roh and J. Kim, *Microchim. Acta*, 2015, **182**, 849–854.
81 S. Evans, A. G. Stuart, J. M. Elliott, L. M. Andrews, P. N. Bartlett, P. J. Doyle and G. Denuault, *Anal. Chem.*, 2002, **74**, 1322–1326.
82 X. L. Luo, J. J. Xu, Y. Du and H. Y. Chen, *Anal. Biochem.*, 2004, **334**, 284–289.
83 D. J. Guo and H. L. Li, *J. Electroanal. Chem.*, 2004, **573**, 197–202.

